Ultrafast fragmentation dynamics of triply charged carbon dioxide: Vibrational-mode-dependent molecular bond breakage

HongJiang Yang,[1,2] Enliang Wang,[3,*] WenXiu Dong,[1,2] Maomao Gong,[1,2] Zhenjie Shen,[1,2] Yaguo Tang,[1,2] Xu Shan,[1,2] and Xiangjun Chen[1,2,†]

[1]*Hefei National Laboratory for Physical Sciences at Microscale and Department of Modern Physics, University of Science and Technology of China, Hefei, Anhui 230026, China*

[2]*Synergetic Innovation Center of Quantum Information and Quantum Physics, University of Science and Technology of China, Hefei, Anhui 230026, China*

[3]*Max-Planck-Institut für Kernphysik, Saupfercheckweg 1, 69117 Heidelberg, Germany*

(Received 4 December 2017; published 4 May 2018)

The *ab initio* molecular dynamics (MD) simulations using an atom-centered density matrix propagation method have been carried out to investigate the fragmentation of the ground-state triply charged carbon dioxide, $CO_2^{3+} \rightarrow C^+ + O_a^+ + O_b^+$. Ten thousands of trajectories have been simulated. By analyzing the momentum correlation of the final fragments, it is demonstrated that the sequential fragmentation dominates in the three-body dissociation, consistent with our experimental observations which were performed by electron collision at impact energy of 1500 eV. Furthermore, the MD simulations allow us to have detailed insight into the ultrafast evolution of the molecular bond breakage at a very early stage, within several tens of femtoseconds, and the result shows that the initial nuclear vibrational mode plays a decisive role in switching the dissociation pathways.

DOI: 10.1103/PhysRevA.97.052703

I. INTRODUCTION

When two or more electrons are removed from a polyatomic molecule by an ultrafast intense laser field, or by bombarding it on the thin solid foil, as well as by collision with an energetic charged particle, the remaining positive molecular ion is usually not stable and will eventually dissociate. The simplest mechanism of fragmentation for multiply charged molecular ions is the single-step Coulomb explosion (CE), in which all bonds break simultaneously and the ionic fragments are driven apart purely by their Coulomb repulsion. By measuring momentum vectors of the fragments in coincidence, the molecular structure can be reconstructed based on the CE picture. The relevant technique, usually referred to as Coulomb explosion imaging (CEI) [1], was used to image the ultrafast dynamical change in the geometry of the molecule in transient state [2–7] or to determine the stereochemical configuration of chiral molecules [8–10]. However, the dynamics of the dissociation of a multiply charged molecular ion is usually very complicated. Recent studies [11–13] on the three-body dissociation of CO_2^{3+} ion by multicoincidence momentum imaging techniques showed that various breakup mechanism scenarios can take place. Besides the direct single-step process where all bonds break simultaneously, CO_2^{3+} ion can also undergo sequential fragmentation, as well as asynchronous dissociation. With the help of potential-energy curves, exploration at the multireference configuration interaction level, Wang *et al.* were able to show that the sequential fragmentation occurs mainly for the ground state ($^2\Pi$) and the first two low-lying electronic excited states ($^4\Pi$ and $^2\Sigma^+$) of the CO_2^{3+} ion [13].

Experimentally, the breakup mechanisms were identified based on the momentum correlation analysis of the ionic fragments using Dalitz plots and Newton diagrams [11–13]. The dynamical behavior at a very early stage within several tens of femtoseconds (fs) should play a decisive role in the dissociation, which experiments cannot tell. Taking the advantage of the latest progress in theoretical methods as well as the ever-increasing computer capacity, it is now possible to model the molecular dynamics (MD) that can reproduce the experimental observables in more detail [14,15]. Large numbers of MD trajectories can be simulated and provide us with not only the information on nuclear motions and other molecular properties at every single time step in each trajectory, but also the statistical information of fragmentation mechanisms, which is more straightforward to compare with the experimental data [16,17].

Here, the *ab initio* MD simulations have been performed to study the fragmentation dynamics of CO_2^{3+} in ground state. Totally 10,000 trajectories have been simulated, and about 27% undergo three-body fragmentation. By analyzing the momentum correlation of the fragments for the three-body events, we can also obtain the Dalitz plot and Newton diagram. The result unambiguously shows that the sequential fragmentation dominates in the three-body dissociation of the ground-state CO_2^{3+}, consistent with our experimental observations by electron impact triple ionization of CO_2. Moreover, the MD simulations allow us to have detailed insight into the ultrafast evolution of the molecular bond breakage at a very early stage, within several tens of femtoseconds. By predetermining the initial nuclear vibrational mode, it is shown that dominantly the asymmetrical stretching vibration leads to

*enliang.wang@mpi-hd.mpg.de
†xjun@ustc.edu.cn

the sequential fragmentation. We demonstrate that the initial nuclear vibrational mode plays a decisive role in switching the dissociation pathways.

II. THEORETICAL METHODS

The *ab initio* molecular dynamics simulation is performed under the extended Lagrangian MD scheme adopting the atom-centered density matrix propagation (ADMP) method [18–20], an alternative approach to the Car-Parrinello molecular dynamics (CPMD) method [21], in which the density matrix elements instead of the molecular orbitals are propagated together with the nuclear degrees of freedom. Different from the CPMD, which is usually carried out by expanding the Kohn-Sham orbitals in a plane-wave basis set, in the ADMP approach the one-electron density matrix is expanded in an atom-centered Gaussian basis and is propagated as electronic variables. Briefly, the nuclear-density matrix system can be described using the extended Lagrangian, which is defined as [18]

$$\mathcal{L} = \tfrac{1}{2}\mathrm{Tr}(\mathbf{V}^{\mathbf{T}}\mathbf{M}\mathbf{V}) + \tfrac{1}{2}\mu\mathrm{Tr}(\mathbf{W}\mathbf{W}) - E(\mathbf{R},\mathbf{P}) - \mathrm{Tr}[\Lambda(\mathbf{P}\mathbf{P}-\mathbf{P})], \quad (1)$$

where $\mathbf{M}$, $\mathbf{R}$, and $\mathbf{V}$ are the nuclear masses, positions, and velocities, respectively, and $\mathbf{P}$, $\mathbf{W}$, and μ are the density matrix, the density matrix velocity, and the fictitious mass for the electronic degrees of freedom, respectively. Idempotency and particle number are conserved by the Lagrangian constraint matrix Λ. Using the principle of stationary action for the Lagrangian in Eq. (1), the Euler-Lagrange equations of motions for the density matrix and the nuclei are

$$\mu\frac{d^2\mathbf{P}}{dt^2} = -\left[\frac{\partial E(\mathbf{R},\mathbf{P})}{\partial \mathbf{P}}\Big|_{\mathbf{R}} + \Lambda\mathbf{P} + \mathbf{P}\Lambda - \Lambda\right], \quad (2)$$

$$\mathbf{M}\frac{d^2\mathbf{R}}{dt^2} = -\frac{\partial E(\mathbf{R},\mathbf{P})}{\partial \mathbf{R}}\Big|_{\mathbf{P}}. \quad (3)$$

The Gaussian basis is used to calculate the energy E and its derivatives $[\partial E(\mathbf{R},\mathbf{P})/\partial\mathbf{P}|_{\mathbf{R}}]$ and $[\partial E(\mathbf{R},\mathbf{P})/\partial\mathbf{R}|_{\mathbf{P}}]$. Equations (2) and (3) can be integrated using the velocity Verlet algorithm [22]. The specific advantages of the ADMP method have been discussed a lot in previous studies [20], briefly, including (i) the freedom to rigorously treat all electrons in the system or to use pseudopotentials; (ii) the capability of using reasonably large time steps through the use of a tensorial fictitious mass with smaller values for the fictitious mass; (iii) a wide variety of accurate and effective exchange-correlation functionals, including hybrid density functionals can be employed; (iv) the ability to treat charged molecular systems and clusters; (v) the deviation from the Born-Oppenheimer surface and the mixing of fictitious and real kinetic energies can be rigorously controlled on-the-fly by choosing the initial condition of the density matrix velocity or using the better way, i.e., obtaining the velocity from converged or approximately converged self-consistent field calculations [19]; and (vi) good computational efficiency.

Before the ADMP simulation, we first analyze the positions and velocities of the three atoms i.e., C and two Os of the neutral CO_2 under room temperature (300 K) using the quasiclassical fixed normal-mode sampling method where the populations

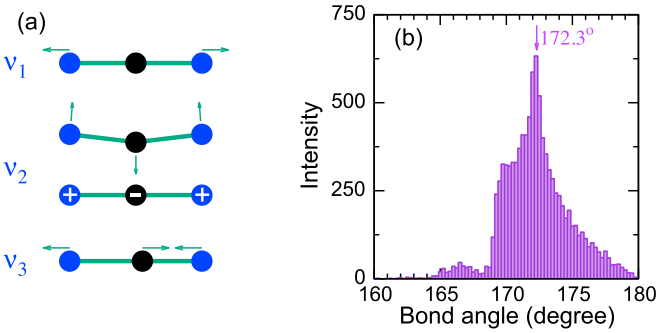

FIG. 1. (a) Vibrational modes of CO_2, and (b) molecular bond angle distribution considering all the vibrational modes.

of the vibrational and rotational states are sampled using Boltzmann distribution. Such a procedure is usually referred to as a thermal sampling process, which simulates the molecular rotation-vibration under certain temperatures. In this work, the vertical transition from neutral CO_2 to the electronic ground state of its trication is assumed to be valid. Thereby, the ADMP simulations can be started from the initial conditions of neutral CO_2 obtained by the thermal sampling process. We first prepare 10,000 initial conditions (nuclear positions and velocities) and then use them as the input parameters for the ADMP simulation, which is carried out using the density-functional theory method, adopting a B3LYP hybrid functional and cc-pVDZ basis set. The fictitious electronic mass is 0.1 amu, and the simulation timescale is 500 fs with a time step of 0.5 fs. For CO_2 molecules, there are four vibration modes involved, as shown in Fig. 1(a), the symmetrical stretching mode ν_1, two degenerated bending modes ν_2, and the asymmetrical stretching mode ν_3. All of the four vibration modes are included in the thermal sampling process. The sampled bond angle distribution of CO_2 at 300 K is shown in Fig. 1(b), which is in good agreement with the result of Siegmann *et al.* [23]. The positions and the velocity vectors of each fragment at each simulation step can be obtained and thus the internuclear distances as well as the three-dimensional momentum vectors of each fragment at each step can be reconstructed. In this work, all the theoretical calculations are performed using the Gaussian package [24].

III. EXPERIMENTAL METHODS

In order to reconfirm the experimental observations, we have carried out new measurements on the three-body fragmentation process $CO_2^{3+} \rightarrow C^+ + O_a^+ + O_b^+$ induced by the collision of 1500-eV electrons using the multicoincidence momentum imaging technique [25]. By analyzing the momentum correlation between the two fragment O^+ ions [13], the events from sequential fragmentation can be extracted. The resulting kinetic energy release (KER) distribution demonstrates again that sequential fragmentation mainly originates from CO_2^{3+} in ground and low-lying electronic states, as discussed in the previous study [13]. In order to investigate the momentum correlation among the three fragments, we employ the Dalitz plot [11,26]. In the Dalitz plot, the difference of the normalized

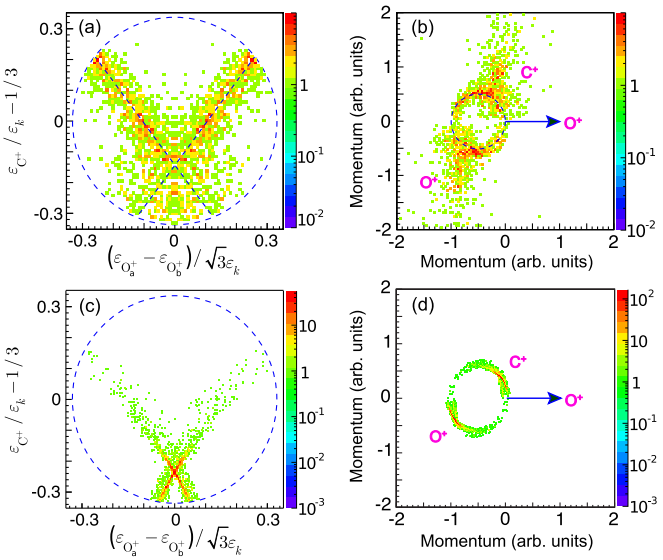

FIG. 2. Experimental and simulated Dalitz plots (left column) and Newton diagrams (right column) for CO_2^{3+}: (a) and (b) for experiment, and (c) and (d) for simulation.

kinetic energy of the two O^+ ions is plotted in the x axis while the normalized kinetic energy of C^+ is plotted in the y axis,

$$x = \frac{\varepsilon_{O_a^+} - \varepsilon_{O_b^+}}{\sqrt{3}\varepsilon_k}, \tag{4}$$

$$y = \frac{\varepsilon_{C^+}}{\varepsilon_k} - \frac{1}{3}, \tag{5}$$

where $\varepsilon_{O_i^+}$ $(i = a,b)$ is the kinetic energy of the oxygen ion, ε_{C^+} is the kinetic energy of the carbon ion, and ε_k is the total kinetic energy. In the Dalitz plot, each point presents a certain momentum correlation among the three fragments [11] at the instance of breakup, e.g., the central bottom point $(0, -1/3)$ indicates the linear fragmentation where the two O^+s are emitted back to back with the C^+ left at rest, and the point near $x = 0$ corresponds to the molecular bending fragmentation where the dissociation is associated with the bending vibration of the molecule. For the sequential fragmentation, these events will scatter on the X-shaped structure on the Dalitz plot [11,13]. In the experiment, we select the events from sequential fragmentation by setting the condition on the momentum correlation spectrum of the two O^+s: for the sequential fragmentation the two O^+s will be produced in two steps and there is no momentum correlation between them. The experimental Dalitz plot for the sequential fragmentation events is given in Fig. 2(a). The plot shows an X-shaped structure marked by the dashed lines, indicating the sequential breakup [11]. The sequential mechanism can be presented more clearly using the Newton diagram. As shown in Fig. 2(b), one of the O^+ ions is fixed on the x axis and its momentum vector is normalized to unit while the C^+ ion and another O^+ ion are plotted on the upper and lower half of the diagram. The circular pattern in the Newton diagram is a direct evidence of the sequential mechanism, i.e., the two C-O bonds break in a stepwise manner. In the first step, the CO_2^{3+} ion dissociates into $O^+ + CO^{2+}$. After a time of delay, when the Coulomb force between O^+ and CO^{2+} is small enough, as the first emitted O^+ fly far away from the CO^{2+} group, the second step occurs: the intermediate CO^{2+} group dissociates into $C^+ + O^+$. Due to the rotation of the intermediate group relative to the first emitted O^+ ion, the circular structure will be presented on the Newton diagram. The jetlike pattern in the Newton diagram is due to the indistinguishable emission of the first and second O^+ ions.

IV. RESULTS AND DISCUSSION

On the MD simulation side, only the ground state of CO_2^{3+}, $^2\Pi$, is considered and the three-body fragmentation events are selected if the internuclear distances between C^+ and any of the two O^+ ions are larger than 10 a.u. at 500 fs. The momentum vectors for the three fragments at 500 fs can be reconstructed for each trajectory. Using the reconstructed momentum vectors for all the simulated three-body events, we can also obtain the simulated Dalitz plot and Newton diagram, which are shown in Figs. 2(c) and 2(d), respectively. The distinct X-shaped structure in the simulated Dalitz plot directly demonstrates the sequential mechanism for the three-body dissociation of the ground-state CO_2^{3+}. We also analyzed the Dalitz plot at different simulation times and it is found that the cross point of the X-shaped structure shifted a little bit to the positive direction of the y axis. The cross point of the X-shaped

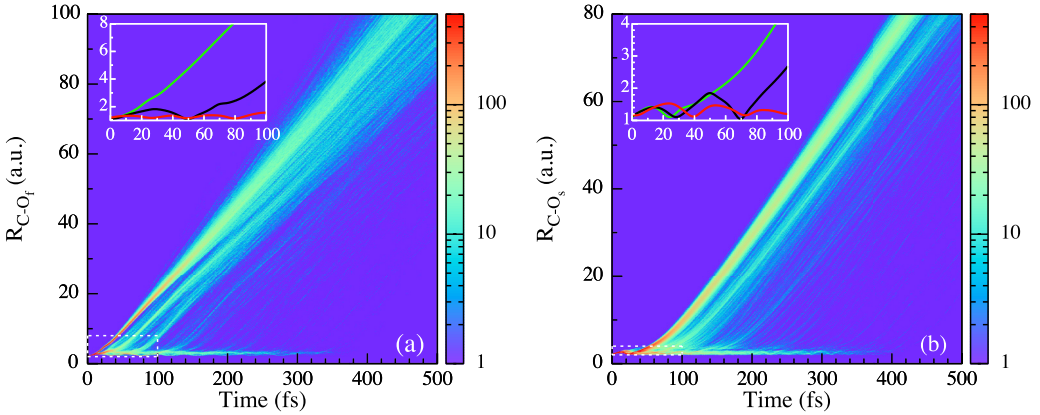

FIG. 3. Distance between the C^+ and O^+ as a function of the evolution time (a) for the first broken C-O_f bond ($R_{C\text{-}O_f}$) and (b) for the second broken C-O_s bond ($R_{C\text{-}O_s}$). The insets show three typical trajectories in 0–100 fs.

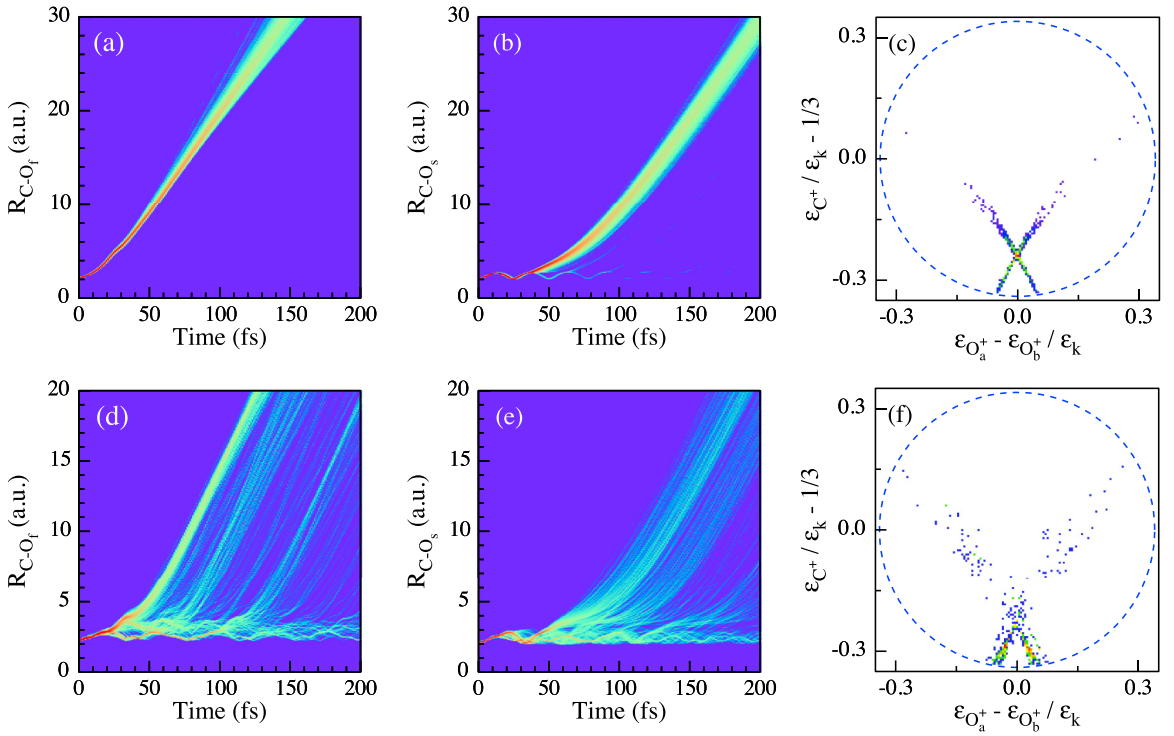

FIG. 4. Simulated initial vibrational mode specified evolution trajectories of the two C-O bonds and their relevant Dalitz plots. For the asymmetrical stretching mode: (a) nuclear distance of the first broken C-O_f bond ($R_{C\text{-}O_f}$) as a function of evolution time, (b) the same for the second broken C-O_s bond ($R_{C\text{-}O_s}$), and (c) the Dalitz plot. For symmetrical stretching mode: (d) $R_{C\text{-}O_f}$ as a function of evolution time, (e) the same for $R_{C\text{-}O_s}$, and (f) the Dalitz plot.

structure is estimated to be (0.00, −0.23) if the simulation time is long enough. For the experimental Dalitz plot, the cross point is located at (0.00 ± 0.12, −0.14 ± 0.12). Considering the uncertainty of the experimental data, the cross point of the simulation agrees with the experiment. The sequential mechanism can be further confirmed by the clear circular pattern in the simulated Newton diagram in Fig. 2(d).

Moreover, the MD simulations allow us to have detailed insight into the ultrafast evolution of molecular bond breakage at a very early stage, within several tens of femtoseconds. Figure 3 plots the simulated trajectories exhibited by the change of nuclear distances of the two C-O bonds as a function of evolution time. Three typical trajectories in 0–100 fs are shown in the insets. The longer and shorter bonds are labeled as C-O_f (refers to the first broken bond) and C-O_s (refers to the second broken bond), respectively. It is shown in Fig. 3(a) that for a considerable part of the events (branch ratio about 42.3%) the C-O_f bond stretches rapidly in the first tens of femtoseconds, and after an inflection point at about 30 fs the C-O_f distance elongates almost linearly with the evolution time, indicating the direct breakage of this bond. The green solid line in the inset of Fig. 3(a) shows the typical trajectory of this mechanism. For other events, on the other hand, the C-O_f bond dissociates at times 20–300 fs after one or more cycles of vibration. The typical trajectories of this mechanism are shown by the solid black line and the solid red line in the inset of Fig. 3(a).

For the C-O_s bond, however, all the events vibrate one or more cycles before dissociation, as shown in Fig. 3(b). An intensive bunch of trajectories shows that the C-O_s bond for a majority of the events vibrates for one and a half cycles during the first 35 fs and then stretches rapidly to dissociate. These events contribute about 41.6% to the total three-body dissociation events, which is very close to the branch ratio of the direct breakage of the C-O_f, indicating that there should be a correlation between the direct dissociation of C-O_f and the breakage of C-O_s with vibrating for one and a half cycles. In the insets of Figs. 3(a) and 3(b), the lines with same color originate from the same molecule. The correlations between the two molecular bonds are clear: (i) the direct dissociation of C-O_f corresponds to the C-O_s vibrations one cycle before dissociation; (ii) if C-O_f vibrates one cycle before dissociation, C-O_s will vibrate more than one cycle; and (iii) both of the two bonds can vibrate several cycles before dissociation.

In order to reveal the reason for the correlation, it is meaningful to predetermine the initial vibrational mode to investigate the fragmentation dynamics in more detail. The results are shown in Fig. 4. By choosing three-body fragmentation events with initial vibration in asymmetrical stretching mode, the evolution trajectories of the two C-O bonds are plotted in Figs. 4(a) and 4(b). It is quite straightforward to see that asymmetrical stretching vibration will lead to sequential fragmentation, where one of the C-O bonds (C-O_f) breaks up directly, and after one and a half cycles (∼35 fs) of vibration another C-O bond (C-O_s) starts to dissociate. This conclusion can further be demonstrated by the clear X-shaped structure in the relevant Dalitz plot in Fig. 4(c). The time of one cycle of C-O_s bond vibration before dissociation can estimated to be 23 fs, which is very consistent with the value estimated from the measured vibrational energy of CO^{2+} in ground state by

threshold photoelectron coincidence spectroscopy [27], indicating that this sequential fragmentation is a clean, two-step process. On the other hand, if we choose the events with initial symmetrical stretching mode, the two C-O bonds will evolve as shown in Figs. 4(d) and 4(e). The two C-O bonds behave quite similarly: each of them undergoes one or more cycles of vibration, leading to the concerted dissociation at times from several tens of femtoseconds to more than 300 fs. The relevant Dalitz plot is drawn in Fig. 4(f). It is shown that almost all the events locate near (0, −0.3), indicating that the two O^+ ions are emitted with almost identical momentum, leaving C^+ at rest, which is the result of the concerted dissociation. The branch ratio of the trajectories of asymmetrical stretching and symmetrical stretching is 2.56:1.00. As for the bending mode, it leads to a deviation of the most probable bond angle from 180°, as shown in Fig. 1(b), but has little influence on the behavior of the fragmentation.

V. CONCLUSIONS

In summary, the *ab initio* MD simulations using the atom-centered density matrix propagation method have been carried out to investigate the fragmentation of ground-state triply charged carbon dioxide. Tens of thousands of trajectories have been simulated until 500 fs and the momentum vectors for the three fragments are reconstructed for each event. By analyzing the momentum correlation of the fragments for the three-body events, the Dalitz plot and Newton diagram are obtained, and the result shows that the sequential fragmentation dominates in the three-body dissociation, consistent with our experimental observations. We also investigate the ultrafast evolution of the molecular bond breakage at a very early stage, within several tens of femtoseconds by the MD simulations. Here we demonstrate that the initial nuclear vibrational mode plays a decisive role in switching the dissociation pathways: the asymmetrical stretching vibration destroying the symmetry of CO_2^{3+} leads to sequential fragmentation, which is dominant in the three-body fragmentation, while symmetrical stretching vibration results in concerted dissociation.

ACKNOWLEDGMENTS

This work is jointly supported by the National Natural Science Foundation of China (Grants No. 11534011, No. 11404317, and No. U1432118) and the National Key Research and Development Program of China (Grant No. 2017YFA0402302). E.W. is grateful for a fellowship from the Alexander von Humboldt Foundation. The numerical calculations in this paper have been done on the supercomputing system in the Supercomputing Center of University of Science and Technology of China.

[1] Z. Vager, R. Naaman, and E. P. Kanter, Science **244**, 426 (1989).
[2] F. Légaré, K. F. Lee, I. V. Litvinyuk, P. W. Dooley, A. D. Bandrauk, D. M. Villeneuve, and P. B. Corkum, Phys. Rev. A **72**, 052717 (2005).
[3] E. Gagnon, P. Ranitovic, X.-M. Tong, C. L. Cocke, M. M. Murnane, H. C. Kapteyn, and A. S. Sandhu, Science **317**, 1374 (2007).
[4] Y. H. Jiang, A. Rudenko, O. Herrwerth, L. Foucar, M. Kurka, K. U. Kühnel, M. Lezius, M. F. Kling, J. van Tilborg, A. Belkacem, K. Ueda, S. Düsterer, R. Treusch, C. D. Schröter, R. Moshammer, and J. Ullrich, Phys. Rev. Lett. **105**, 263002 (2010).
[5] I. Bocharova, R. Karimi, E. F. Penka, J.-P. Brichta, P. Lassonde, X. Fu, J.-C. Kieffer, A. D. Bandrauk, I. Litvinyuk, J. Sanderson, and F. Légaré, Phys. Rev. Lett. **107**, 063201 (2011).
[6] H. Ibrahim, B. Wales, S. Beaulieu, B. E. Schmidt, N. Thiré, E. P. Fowe, É. Bisson, C. T. Hebeisen, V. Wanie, M. Giguére, J.-C. Kieffer, M. Spanner, A. D. Bandrauk, J. Sanderson, M. S. Schuurman, and F. Légaré, Nat. Commun. **5**, 4422 (2014).
[7] C. E. Liekhus-Schmaltz, I. Tenney, T. Osipov, A. Sanchez-Gonzalez, N. Berrah, R. Boll, C. Bomme, C. Bostedt, J. D. Bozek, S. Carron, R. Coffee, J. Devin, B. Erk, K. R. Ferguson, R. W. Field, L. Foucar, L. J. Frasinski, J. M. Glownia, M. Gühr, A. Kamalov *et al.*, Nat. Commun. **6**, 8199 (2015).
[8] M. Pitzer, M. Kunitski, A. S. Johnson, T. Jahnke, H. Sann, F. Sturm, L. P. H. Schmidt, H. Schmidt-Böcking, R. Dörner, J. Stohner, J. Kiedrowski, M. Reggelin, S. Marquardt, A. Schiesser, R. Berger, and M. S. Schöffler, Science **341**, 1096 (2013).
[9] M. Pitzer, G. Kastirke, M. Kunitski, T. Jahnke, T. Bauer, C. Goihl, F. Trinter, C. Schober, K. Henrichs, J. Becht, S. Zeller, H. Gassert, M. Waitz, A. Kuhlins, H. Sann, F. Sturm, F. Wiegandt, R. Wallauer, L. P. H. Schmidt, A. S. Johnson *et al.*, Chem. Phys. Chem. **17**, 2465 (2016).
[10] P. Herwig, K. Zawatzky, M. Grieser, O. Heber, B. Jordon-Thaden, C. Krantz, O. Novotny, R. Repnow, V. Schurig, D. Schwalm, Z. Vager, A. Wolf, O. Trapp, and H. Kreckel, Science **342**, 1084 (2013).
[11] N. Neumann, D. Hant, L. P. H. Schmidt, J. Titze, T. Jahnke, A. Czasch, M. S. Schöffler, K. Kreidi, O. Jagutzki, H. Schmidt-Böcking, and R. Dörner, Phys. Rev. Lett. **104**, 103201 (2010).
[12] C. Wu, C. Wu, D. Song, H. Su, Y. Yang, Z. Wu, X. Liu, H. Liu, M. Li, Y. Deng, Y. Liu, L.-Y. Peng, H. Jiang, and Q. Gong, Phys. Rev. Lett. **110**, 103601 (2013).
[13] E. Wang, X. Shan, Z. Shen, M. Gong, Y. Tang, Y. Pan, K.-C. Lau, and X. Chen, Phys. Rev. A **91**, 052711 (2015).
[14] P. López-Tarifa, M.-A. Hervé du Penhoat, R. Vuilleumier, M.-P. Gaigeot, I. Tavernelli, A. Le Padellec, J.-P. Champeaux, M. Alcamí, P. Moretto-Capelle, F. Martín, and M.-F. Politis, Phys. Rev. Lett. **107**, 023202 (2011).
[15] M. E.-A. Madjet, O. Vendrell, and R. Santra, Phys. Rev. Lett. **107**, 263002 (2011).
[16] J. Cao, Z. Zhang, C. Zhang, K. Liu, M. Wang, and W. Bian, Proc. Natl. Acad. Sci. U.S.A. **106**, 13180 (2009).
[17] Z. Li, L. Inhester, C. Liekhus-Schmaltz, B. F. E. Curchod, J. W. Snyder, N. Medvedev, J. Cryan, T. Osipov, S. Pabst, O. Vendrell, P. Bucksbaum, and T. J. Martinez, Nat. Commun. **8**, 453 (2017).
[18] H. B. Schlegel, J. M. Millam, S. S. Iyengar, G. A. Voth, A. D. Daniels, G. E. Scuseria, and M. J. Frisch, J. Chem. Phys. **114**, 9758 (2001).
[19] S. S. Iyengar, H. B. Schlegel, J. M. Millam, G. A. Voth, G. E. Scuseria, and M. J. Frisch, J. Chem. Phys. **115**, 10291 (2001).

[20] H. B. Schlegel, S. S. Iyengar, X. Li, J. M. Millam, G. A. Voth, G. E. Scuseria, and M. J. Frisch, J. Chem. Phys. **117**, 8694 (2002).
[21] R. Car and M. Parrinello, Phys. Rev. Lett. **55**, 2471 (1985).
[22] W. C. Swope, H. C. Andersen, P. H. Berens, and K. R. Wilson, J. Chem. Phys. **76**, 637 (1982).
[23] B. Siegmann, U. Werner, H. O. Lutz, and R. Mann, J. Phys. B **35**, 3755 (2002).
[24] M. J. Frisch, G. W. Trucks, H. B. Schlegel, G. E. Scuseria, M. A. Robb, J. R. Cheeseman, G. Scalmani, V. Barone, B. Mennucci, G. A. Petersson, H. Nakatsuji, M. Caricato, X. Li, H. P. Hratchian, A. F. Izmaylov, J. Bloino, G. Zheng, J. L. Sonnenberg, M. Hada, M. Ehara *et al.*, Gaussian 09 Revision B.01 (Gaussian Inc. Wallingford, CT, 2010).
[25] E. Wang, X. Shan, Y. Shi, Y. Tang, and X. Chen, Rev. Sci. Instrum. **84**, 123110 (2013).
[26] R. H. Dalitz, Philos. Mag. **44**, 1068 (1953).
[27] G. Dawber, A. G. McConkey, L. Avaldi, M. A. MacDonald, G. C. King, and R. I. Hall, J. Phys. B **27**, 2191 (1994).